

Sixton rectangles in the structure of alumina ultrathin films on metalsG. Prévot,^{1,*} A. Naitabdi,^{1,2} R. Bernard,¹ and Y. Borensztein¹¹*Institut des NanoSciences de Paris, UMR CNRS 7588, Université Pierre et Marie Curie-Paris 6, 140 rue de Lourmel, 75015 Paris, France*²*Laboratoire de Réactivité de Surface, UMR CNRS 7197, Université Pierre et Marie Curie-Paris 6, 4 place Jussieu, 75252 Paris Cedex 05, France*

(Received 10 November 2009; revised manuscript received 12 January 2010; published 1 February 2010)

In situ room temperature scanning tunneling microscopy (STM) observations combined with low energy electron diffraction and Auger electron spectroscopy were performed to investigate the structure of a thin aluminum oxide film grown on Ni(111). Well-ordered alumina films were obtained after the deposition of 2.5 ML of aluminum on a clean Ni(111) surface, followed by its oxidation under O₂ flow and subsequent annealing at 1000 K. Whereas an hexagonal unit cell corresponding to a $(5\sqrt{3} \times 5\sqrt{3})$ reconstruction with respect to the Ni(111) surface had been previously ascribed to this superstructure, our results indicate that the unit cell corresponds to a sixton rectangle, i.e., a rectangle with a $\sqrt{3}$ ratio between the lengths of the two sides of the mesh (18.2×10.5 Å²). We attribute this specific ratio to the presence of the hexagonal arrangement of an oxygen plane in the layer. From the size and aspect ratio of the mesh and from the STM observations, we also conclude that the atomic organization observed for alumina/Ni(111) is very similar to the organization observed for alumina grown on FeAl(110), NiAl(110), Cu-9 at. % Al(111), and Cu(111), which provides strong argument that this alumina structure is not specific of aluminum-based substrates but could be the equilibrium state of a two-layers-thick alumina film on a metal.

DOI: [10.1103/PhysRevB.81.085405](https://doi.org/10.1103/PhysRevB.81.085405)

PACS number(s): 68.37.-d, 68.55.-a, 68.47.Gh

I. INTRODUCTION

Ultrathin oxide layers on metallic substrates play a key role in many applications and are widely studied.^{1,2} Among them, alumina layers have attracted great interest due to the fact that crystalline layers with a well-defined nanometric thickness can be easily prepared. In addition, because of their remarkable stability and their complex physical properties, these systems have attracted widespread interest in the field of heterogeneous catalysis on oxide-supported metal nanoparticles.³ In particular, the structural arrangement of alumina surface has been used as a template for the growth of size-controlled self-assembled metal nanoparticles.^{4,5} For such a growth, oxygen vacancies at the domain boundaries have been shown to act as preferential adsorption sites for metal atoms.^{5,6} Interesting physical phenomena have been reported on oxide-supported metal clusters,⁷ including charge transfer to metal nanoclusters through the thin oxide film, activated by a decrease in the work function of the metal substrate at the metal-oxide interface in combination with the electronegativity of the adsorbates.⁸

Alumina films are generally prepared by oxidation of aluminum alloys or aluminum films, followed by annealing in the 800–1200 K temperature range. Depending on the substrate and preparation conditions, various alumina structures have been obtained. If 10 Å thick films have been grown on NiAl(100) (Ref. 9) and CoAl(100),¹⁰ and were attributed to a θ -Al₂O₃ structure, alumina films have generally a smaller thickness around 5–8 Å. The structure of these thinner films is based on two compact oxygen planes with a more or less local hexagonal arrangement and with an atomic density close to the density of (111) planes in γ -Al₂O₃ or of (0001) planes in α -Al₂O₃. The local hexagonal order in the layers generally gives rise to spots of high intensity in the diffrac-

tion patterns.^{11–15} The lattice constant associated to this short-range hexagonal organization ranges between 2.8 and 3.1 Å. The lowest values are generally found for thicker films and low annealing temperature T_A . They are close to the mean O-O distance in the (111) planes of γ alumina (2.7 Å) or in the (0001) planes in α alumina (2.8 Å). The highest values are found for thinner films and high T_A . These high values show that the structure of ultrathin alumina films could strongly differ from the structure of bulk alumina phases. The variation in this O-O distance has been studied, for example, for alumina films grown on Ni₃Al(001). It increases from 2.91 Å for $T_A=900$ K up to 2.99 Å for $T_A=1000$ K.¹⁵ If diffraction by poorly ordered films gives only rise to spots related to this short-range hexagonal organization,¹³ well-ordered films exhibit larger unit cells, either hexagonal [for example, on Ni₃Al(111) (Ref. 16)] or rectangular, which can be slightly distorted [for example on NiAl(110) (Ref. 17)].

Despite the large number of studies performed on these systems, the atomic structure of the alumina layers, and even the superstructure indexation, the electronic structure, the stoichiometry and the origin of the epitaxial relations observed are known for limited cases. The most quantitative results have been obtained for aluminum oxide on NiAl(110), for which numerous studies have been undertaken.^{17–22} Using scanning tunneling microscopy (STM) observations combined with density-functional theory (DFT) calculations, Kresse *et al.* have proposed a structural model which also fits previous x-ray diffraction results²² and is in good agreement with frequency modulation dynamic force microscopy (FM-DFM) observations which have been done more recently.²¹ It is made of an interfacial Al₁₆O₂₄ plane and an Al₂₄O₂₈ surface plane. The atomic arrangement has been described as specific to the NiAl(110) substrate, in particular, for the interface plane, where the pentagon-

heptagon organization of Al atoms is claimed to be due to a preferred chemical short-range order favoring Al-Ni neighbors. However, a similar organization has been observed recently for alumina grown on Cu-9 at. % Al(111),²³ in which the Al atoms of the substrate are expected to play a minor role. For alumina on Ni₃Al(111), that forms a $\sqrt{67} \times \sqrt{67} R47.784^\circ$ superstructure,²⁴ the exact composition of the film has also been recently solved by DFT calculations combined with a STM study,²⁵ indicating a Al₂O_{2.4875} composition. Alumina on NiAl(110) and Ni₃Al(111) surfaces displays a very similar local atomic organization, but in the later case, holes are present in the film structure and act as preferential nucleation sites for Pd atoms.²⁵

In order to clarify the influence of the substrate on the organization of the alumina layer, and especially of the presence of Al atoms, we have investigated the structure of an ultrathin aluminum oxide layer grown on a Ni(111) surface. This choice has been motivated by the fact that such films, prepared at a relatively high annealing temperature (1000 K), have a very good crystalline order.²⁶ Moreover, their composition has been precisely determined, which is possible because no O or Al atoms are present in the Ni(111) substrate.²⁶ By nuclear resonance analysis (NRA), it was found that the aluminum and oxygen densities in the alumina layer are equal to $\theta_{\text{Al}} = (2.3 \pm 0.3) \times 10^{15}$ atom/cm² and $\theta_{\text{O}} = (3.3 \pm 0.3) \times 10^{15}$ atom/cm², respectively.²⁶ This corresponds to an Al₂O₃ composition and to two oxygen compact planes in bulk alumina. This structure was previously indexed as $5\sqrt{3} \times 5\sqrt{3}$ (Ref. 26) but some aspects of the low-energy electron diffraction (LEED) pattern seemed to us to be inconsistent with an hexagonal symmetry, as we will discuss in the next section.

We have used STM, LEED, and Auger electron spectroscopy (AES) to investigate alumina/Ni(111) films. The experimental details and results are described in Sec. II whereas Sec. III is devoted to a general discussion and a comparison with other systems.

II. EXPERIMENTAL RESULTS

Experiments were performed in a UHV system with a base pressure of 5×10^{-11} mbar, equipped with an Omicron variable temperature STM, a SPECS LEED/Auger apparatus, and standard Omicron evaporators. The alumina/Ni(111) layer was prepared using exactly the same procedure as described in Ref. 26. The Ni crystal was cleaned by several cycles of Ar ion sputtering followed by annealing at 1000 K. A 2.5-monolayer- (ML-) thick Al film was deposited on clean Ni(111) at 130 K and annealed at 600 K. During the annealing, a thin epitaxial Ni₃Al(111) film formed.²⁷ The sample was then oxidized at room temperature (RT) during 20 min under 10^{-6} mbar oxygen and further annealed at 1000 K. After this procedure, the surface displayed a very high crystalline order, as it could be seen from the LEED observations (see Fig. 1).

Figure 1 displays the LEED diagram obtained at 90 eV, which is similar to the LEED diagram shown in Ref. 26. In their study of alumina films on Ni(111), Le Pevedic *et al.*²⁶ have attributed the diffraction spots to a $5\sqrt{3} \times 5\sqrt{3}$ commensurate

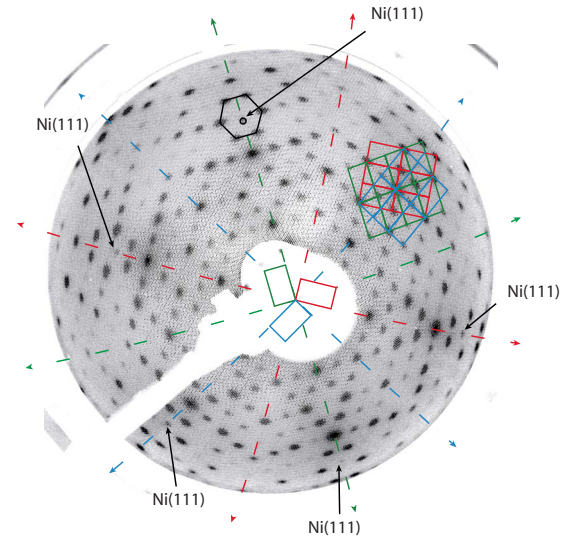


FIG. 1. (Color online) LEED diagram (90 eV) of the $10.5 \times 18.2 \text{ \AA}^2$ superstructure with three equivalent domains. The unit cell of each domain is drawn at the center of the figure. The superposition of the three domains is also given, showing that every fourth spot is common to the three domains. The black arrows indicate the diffraction spots of the Ni(111) substrate, which are only visible at specific energies. The position of the Ni(111) spots with respect to the superstructure spots is enlightened in the hexagon drawn in the upper part of the figure. Along the main axes, indicated by dashed lines, every two spots is missing.

surate superstructure. In fact, an accurate analysis of the LEED pattern shows that this superstructure is not commensurate with the substrate. At specific energies, such as 90 eV, spots related to the Ni(111) crystalline structure are visible. They are indicated by black arrows in Fig. 1. These spots are not at the center of the six nearest spots corresponding to the diffraction by the superstructure (a regular hexagon based on the position of these spots is drawn in Fig. 1 for clarity). A comparison between the position of the spots corresponding to the superstructure and the position of the spots corresponding to Ni(111) indicates that the $5\sqrt{3} \times 5\sqrt{3}$ superstructure cell would be in fact $2.5 \pm 0.5\%$ contracted with respect to the substrate. By partially covering the Ni(111) with Al, we have ensured that the spots attributed to Ni(111), which are only visible at specific energies, really correspond to the diffraction by the substrate. In that case, the alumina film does not cover the whole surface, and bare Ni(111) regions can be directly used as a precise reference for the LEED analysis.

Moreover, along the six main axes (dashed lines), every even spot is missing. Such extinctions are generally characteristic of the pgg symmetry in a rectangular mesh, and cannot be found in an hexagonal mesh. Thus, the diffraction spots should be attributed to a rectangular mesh ($18.2 \times 10.5 \text{ \AA}^2 R0^\circ$), with three equivalent domains rotated by 120° . In the LEED diagram, every fourth spot is common to the three domains. This indicates that the ratio of the lengths of the unit cell is almost exactly $\sqrt{3}$, i.e., the same ratio as for the rectangle inscribed in a regular hexagon, known as sixton rectangle.²⁸

After each step of the growth process (substrate cleaning, Al deposition, NiAl alloy formation, oxidation, and anneal-

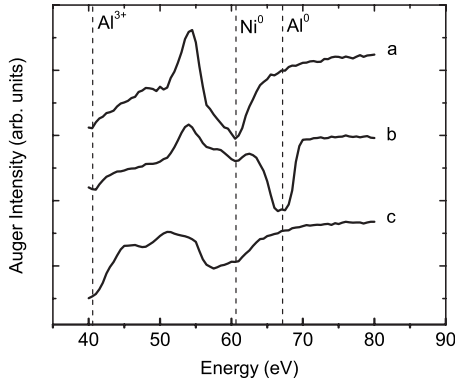


FIG. 2. AES differentiated spectra recorded at RT giving the evolution of the Ni^0 peak area at different steps of the preparation of the alumina film on Ni(111). (a) Clean Ni(111). (b) Thin Al/Ni(111) film right after the deposition of 2.5 ML of aluminum at 150 K. (c) Ultrathin alumina film on Ni(111) obtained after the oxidation at RT of the previous Ni_3Al (111)/Ni(111) and annealing at 1000 K.

ing), AES was performed in order to monitor the evolution of the surface. The Auger spectra obtained after annealing are similar to the spectra shown in Ref. 26 (see Fig. 2). We have particularly checked that annealing the sample after oxidation leads to the diffusion of excess Al atoms deep into the bulk. This ensured that after this final annealing, the alumina film was lying on a pure Ni(111) surface, in agreement with Ref. 26. Figure 2 shows indeed the evolution of the Ni and Al peaks at three stages of the alumina preparation procedure. Spectrum (a), recorded on clean Ni(111) surface prior to Al deposition, shows the Ni^0 peak at 61 eV corresponding to Ni MVV transition. After the deposition of 2.5 ML of aluminum at 150 K, spectrum (b) also displays a peak at 68 eV, related to Al^0 , and corresponding to the Al LVV transition. Spectrum (c), recorded after the formation of the alumina film, indicates the lack of the Al^0 peak. The peak at lower energy can be attributed to oxidized aluminum.

STM experiments were performed at room temperature. The alumina/Ni(111) surface displayed large flat terraces, of about 50-nm average size, separated by monoatomic steps [see Fig. 3(a)] and a few vacancy islands. We think that, depending on the tip condition, we either probed in the same area the hexagonal mesh of the Ni(111) surface through the alumina layer or the alumina layer structure itself with sublattice resolution. The former case is presented in Fig. 3(b). The Ni(111) lattice is very regular and the atoms appear not to be affected by the alumina layer. The corresponding hexagonal atomic structure displays an interatomic distance, $d_{\text{Ni-Ni}} = 2.5 \text{ \AA}$ equal to the same distance on clean Ni(111). This is in good agreement with ion channelling experiments which have shown that the relaxation of substrate atoms due to the alumina film were negligible.²⁶ Similar observations of the underlying metallic substrate by tunneling through the alumina layer have been also reported for alumina/TiAl(111).²⁹ Because of the homogeneity of our alumina layer, it seems likely that we observed the Ni(111) surface through the alumina layer. However we cannot exclude the fact that the position of the tip apex has changed toward a hole in the film or the film has been moved by the tip,

exposing the bare substrate. The large scale view of the surface in Fig. 3(c) corresponds to the latter case, i.e., the observation of the alumina layer. Large domains appear as stripes on the alumina film and different orientations are visible. The size of the domains is on the order of few tens of nanometers with an average size equal to 60 nm. Two types of domain boundaries can be distinguished between two adjacent domains on our alumina film. The first ones correspond to reflection domain boundaries which separate areas of different orientations [see the dotted arrow in Fig. 3(c)] whereas the second ones are antiphase domains and are related to lines separating domains of the same orientation [see solid arrow in Fig. 3(c)]. A detailed view of the boundary between two domains of different orientation is shown in Fig. 3(d), where the lattice unit cells of the two domains have been superimposed. The line defects between reflection domains appear irregular and are due to the atomic arrangement in the alumina film along two different planes. The second line defects appear straight and uniform. The presence of similar two line defects has been also observed for alumina films on NiAl(110).³⁰ The electronic properties of antiphase domain boundaries have been investigated thoroughly by Nilius *et al.*³¹ using scanning tunneling microscopy and spectroscopy. The authors attributed the high electron density contrasts to three unoccupied states originating from a non-stoichiometric alumina composition between the two domains. However, only reflection domain boundaries were observed for alumina films on Cu-9 at. % Al(111).²³

A STM high-resolution image of the superstructure is shown in Fig. 4(a). The structure really corresponds to a rectangular unit cell with pgg symmetry. This sublattice resolution image shows that protrusions are arranged either in pentagons or in elongated rectangles. Our STM observations are very similar to STM results obtained for alumina grown on Cu-9 at. % Al(111) (Ref. 23) and NiAl(110).¹⁷ For alumina grown on NiAl(110), the atomic structure has been precisely determined by *ab initio* simulations and the bright spots observed under such tunneling conditions have been attributed to aluminum atoms located at the interface with the substrate.¹⁷ A schematic of the corresponding interfacial alumina plane and of the alumina surface plane is given in Figs. 4(c) and 4(d), together with a schematic of the Ni(111) surface plane at the same scale. The superimposition, in the STM image of Fig. 4(a), of the interface Al atoms from the model given by Kresse *et al.* for alumina on NiAl(110) shows that the protrusions that we observe are likely to be attributed to Al interface atoms arranged in the same way as for alumina on NiAl(110), with a number of 16 atoms per unit cell.

For alumina/Cu-9 at. % Al(111), two different superstructures have been identified, showing a very similar mesh, but displaying a different relationship with the substrate. Since STM images were similar to those obtained on alumina/NiAl(110), the structure was described as identical to the one proposed by Kresse *et al.* In the following, we will discuss if the same results apply for alumina/Ni(111).

III. DISCUSSION

The numbers N_{Al} and N_{O} of Al and O atoms per unit cell can be inferred from the measurements of the Al and O con-

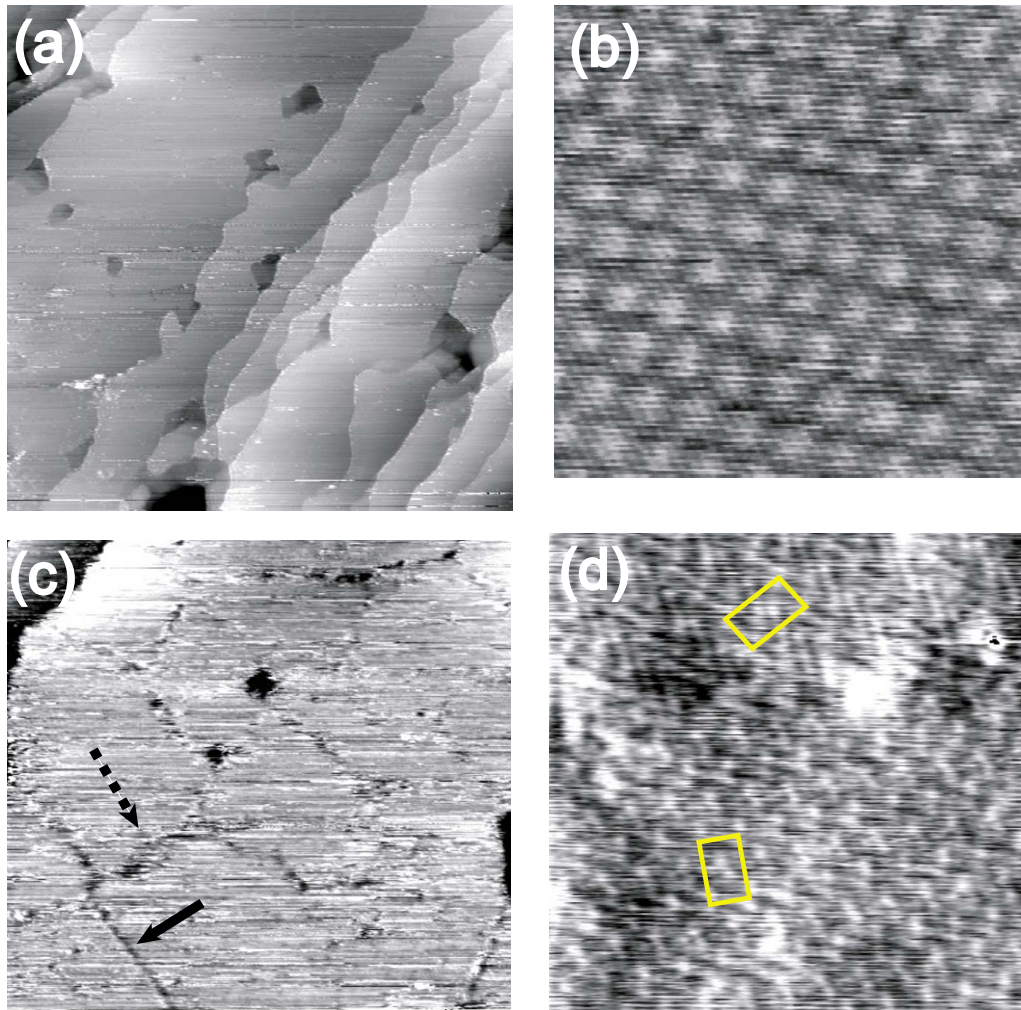


FIG. 3. (Color online) STM images of the alumina layer on Ni(111). (a) $440 \times 440 \text{ nm}^2$, $U = -4 \text{ V}$, and $I = 0.1 \text{ nA}$. (b) Atomic-resolution STM image, $2.5 \times 2.2 \text{ nm}^2$, corresponding to $U = 0.3 \text{ V}$, $I = 1.2 \text{ nA}$, showing the Ni(111) atoms by tunneling through the alumina layer. (c) $150 \times 140 \text{ nm}^2$, $U = 2.3 \text{ V}$, and $I = 0.15 \text{ nA}$. The two types of domain boundaries present on the alumina film are indicated with two arrows (see text). (d) High-resolution $13 \times 13 \text{ nm}^2$ STM image showing a boundary between two domains of different orientation. The unit cell of the different domains is indicated by yellow rectangles. $U = 2.5 \text{ V}$ and $I = 0.19 \text{ nA}$.

ment in the layer.²⁶ The values derived are $N_{\text{Al}} = 44 \pm 6$ and $N_{\text{O}} = 63 \pm 6$, thus corresponding to a stoichiometric alumina layer. In contrast, for alumina/NiAl(110), the atomic composition differs from the 2/3 ratio between aluminum and oxygen atoms. Kresse *et al.* have proposed a model of a quasi-rectangular unit cell for which $N_{\text{Al}} = 40$ and $N_{\text{O}} = 52$. The number of aluminum atoms is compatible with the value found for alumina/Ni(111) but the number of oxygen atoms is significantly smaller.

However, although the oxygen content in the alumina film on Ni(111) is different from the *ab initio* predictions for alumina on NiAl(110), the size of the mesh and the STM observations are very similar for these two superstructures. More precisely, the STM images that we observed for alumina on Ni(111) are very similar to STM images in which the bright spots were attributed to interface Al atoms for aluminum oxide on the NiAl(110) surface.¹⁷ We undoubtedly observe the same atoms. This means that the same organization of interface Al atoms can be obtained for two substrates displaying a completely different structure. The only notice-

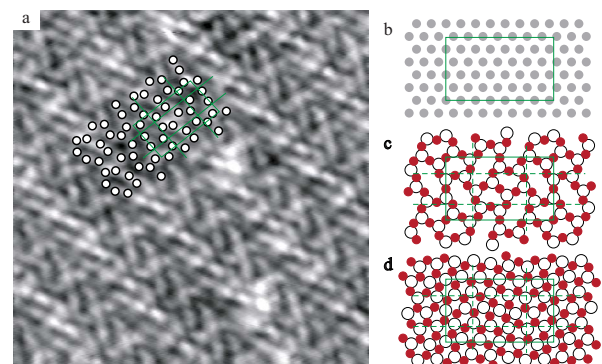


FIG. 4. (Color online) (a) STM image of the alumina layer. $8.8 \times 8.8 \text{ nm}^2$, $U = 0.3 \text{ V}$, and $I = 1 \text{ nA}$. [(b)–(d)] Schematic of (b) the Ni(111) substrate, (c) the interfacial layer, (d) the surface layer derived from the superstructure of alumina/NiAl(110). Grey dots: Ni atoms and black circles: Al atoms. Red dots: oxygen atoms. The rectangle corresponds to the alumina unit cell and dotted lines to the glide planes.

TABLE I. Geometrical characteristics of the alumina superstructures observed on various substrates and displaying a rectangular or nearly rectangular unit cell with an aspect ratio close to $\sqrt{3} \approx 1.73$. The number of domains observed and the preparation temperature are also given.

Substrate	Superstructure	Ratio	Domains	Preparation temperature(K)	Reference
Ni(111)	$18.2 \times 10.5 \text{ \AA}^2$ $\gamma=90^\circ$	1.73	$R0^\circ$, 3	1000	This work
NiAl(110)	$18.01 \times 10.59 \text{ \AA}^2$ $\gamma=91.15^\circ$	1.70	$R \pm 24.01^\circ$, 2	1070	22
FeAl(110)	$18.2 \times 10.7 \text{ \AA}^2$ $\gamma=91^\circ$	1.70	$R \pm 24^\circ$, 2	1123	32
Cu(111)	$17.6 \times 10.1 \text{ \AA}^2$ $\gamma=90^\circ$	1.74	$R \pm 22.5^\circ$, 6	1200	11
Cu-9 at. % Al(111)	$18.2 \times 10.6 \text{ \AA}^2$ $\gamma=90^\circ$	1.72	$R30^\circ$, 3	953	23
	$18.3 \times 10.6 \text{ \AA}^2$ $\gamma=90^\circ$	1.73	$R \pm 18^\circ$, 6		

able influences of the substrate are a slight distortion of the mesh (our mesh is rectangular whereas the angle between the two sides of the mesh on NiAl(110) is 91.15°) and of course, a different number of domain orientations, due, in particular, to a different substrate symmetry. The structure of alumina observed on NiAl(110) is therefore not specific of aluminum-based alloys and can also be observed on aluminum free single metals such as Ni(111). In their study of alumina/NiAl(110), Kresse *et al.* attributed the heptagon and pentagon organizations at the interface to the Al-Al repulsion between Al atoms from the interface and Al atoms from the substrate. Our experiments show that this cannot be involved in the structure formation since no Al atoms are present in the substrate. The small difference between the structures of alumina/NiAl(110), alumina/Cu-9 at. % Al(111), and alumina/Ni(111) is the distortion of the unit cell. For alumina/NiAl(110), the cell dimensions are $18.01 \times 10.59 \text{ \AA}^2$, with an angle of $\gamma=91.15^\circ$. On the contrary, for alumina/Cu-9 at. % Al(111) and alumina/Ni(111) the cell is rectangular ($18.2 \times 10.6 \text{ \AA}^2$), and the aspect ratio of the rectangle is $\sqrt{3}$. Note that the aspect ratio in the case of alumina/NiAl(110) is very close to $\sqrt{3}$ too. These differences could be attributed to the fact that the distortion of the alumina/NiAl(110) cell yields a matching between Ni[$1\bar{1}0$] rows and Al pseudorows of the interface plane, needed by the strong Al-Al repulsion, whereas for Cu-9 at. % Al, the Al atomic fraction near the surface is too small to drive the morphology of the unit cell and, for Ni(111), no Al is present in the substrate.

We have explored previous reports in the literature to check if this alumina superstructure could be present for other systems. Two systems, for which, to our knowledge, no STM studies have been performed, display diffraction patterns that could be attributed to a similar alumina structure: alumina/FeAl(110) (Ref. 32) and alumina/Cu(111).¹¹ Alumina/FeAl(110) displays almost the same LEED diagram as alumina/NiAl(110). Its structure can thus be described by a quasirectangular unit cell, of size around $10.5 \times 18 \text{ \AA}^2$, and with the *pgg* symmetry.³² Alumina/Cu(111) displays a more complex LEED diagram,¹¹ that we carefully analyzed. The diagram presented by Jeliazova and Franchy can be ascribed to a rectangular unit cell of dimensions around $10 \times 18 \text{ \AA}^2$ with six domain orientations at $\pm 22.5^\circ$ from the main axes of the surface and having a *pgg* symmetry. STM experiments

on this system would be of great interest. The different substrates for which alumina grows with such rectangular unit cell are listed in Table I. For all these cases, the temperature at which the alumina is prepared is relatively high, i.e., in the 950–1200 K temperature range. This indicates that the structures obtained are very stable. In particular, for alumina/Cu-9 at. % Al(111), oxidation at lower temperature leads to a different film structure which is indexed as $7\sqrt{3} \times 7\sqrt{3}R30^\circ$.²³ The alumina/Ni₃Al(111) film, prepared in the 1000–1100 K temperature range, appears to be, with its specific $\sqrt{67} \times \sqrt{67}R47.784^\circ$ superstructure, an exception to the sixton structure.^{24,25}

What could be the origin of such a sixton superstructure? The ratio between the lengths of the two sides of the meshes of alumina grown on NiAl(110),¹⁷ Cu(111),¹¹ Cu-9 at. % Al(111),²³ and FeAl(110) (Ref. 32) are listed in Table I. All structures are approximately sixton rectangles, i.e. rectangles with a $\sqrt{3}$ ratio between the lengths of their two sides. This ratio implies that the mesh has the dimensions of a rectangle inscribed in a regular hexagon. For alumina/Ni(111), the sixton structure of the mesh would be easily understood if the superstructure was commensurate with the substrate: in that case, this $\sqrt{3}$ ratio would be needed for matching rectangles on the regular hexagons of the Ni(111) surface. However, the alumina film is not commensurate with the substrate since the larger side of the alumina mesh corresponds to 7.3 Ni interatomic spacings along [$1\bar{1}0$]. For alumina on Cu(111), the domains are rotated by $\pm 22.5^\circ$ so that no specific $\sqrt{3}$ ratio can be attributed to the influence of the substrate. A possible influence of the substrate for fixing the aspect ratio of the mesh to $\sqrt{3}$ can only be found on the first superstructure of alumina on Cu-9 at. % Al(111), which is nearly commensurate with the substrate, and where the domains are oriented along the main crystallographic axes of the surface.²³

The $\sqrt{3}$ ratio can be understood by considering the structure proposed by Kresse *et al.*¹⁷ for an aluminum oxide film on NiAl(110). The structure for the unit cell is a stacking sequence of four planes (see Fig. 4): 16 interface Al atoms (Al_i) lying on the substrate, 24 interface O atoms (O_i), 24 surface Al atoms (Al_s), and 28 surface O atoms (O_s). The two intermediate planes (Al_s and O_i) have the same distorted hexagonal structure with Al atoms located on top of O atoms. We can easily understand that if the hexagons were not dis-

torted, the ratio between the two sides of the rectangle would be $\sqrt{3}$. The fact that this ratio is preserved even when the hexagonal structure is distorted implies that, when averaged over the superstructure unit cell, this distortion conserves the proportions of the regular hexagon. Although we did not observe the presence of the hexagonal structure of Al_s and O_i planes in our STM images (we only observe the Al_i plane), this $\sqrt{3}$ ratio is a strong argument for the presence of such a structure inside our alumina layer.

Moreover, this indicates that we should have 16 interface Al atoms (Al_i) and 24 interface O atoms (O_i) in the alumina/Ni(111) unit cell. From our mesh dimensions, we can conclude that the average O-O nearest-neighbor distance in the distorted hexagonal structure is 3.0 Å, which is in good agreement with other observations on ultrathin alumina layers on various substrates. Thus, the atomic composition of our structure determined by NRA implies that the number of Al atoms in the surface layer would be $44 \pm 6 - 16 = 28 \pm 6$, which is compatible with the number proposed by Kresse *et al.*¹⁷ for Al_s atoms in the alumina/NiAl(110) unit cell. The number of O atoms in the surface layer would however be 39 ± 6 , a value significantly higher than the one predicted for O_s atoms in the alumina/NiAl(110) unit cell.¹⁷ At this stage, we can only conclude that either the two superstructures have not the same O content at the surface, or the O quantity was underestimated in DFT calculations on NiAl(110), or the O quantity was overestimated in the NRA measurements, for example, due to a small amount of oxygen that would be present in the Ni substrate and would thus contribute to the detected signal.²⁶ Note that oxygen underestimation in the surface layer, in DFT calculations, seems unlikely due to the very good agreement with atomic force microscopy (FM-DFM) (Ref. 21) and STM (Ref. 17) observations of the oxygen atoms at the surface.

IV. CONCLUSIONS

In this work, we have studied the structure of an alumina film grown on Ni(111) to investigate the effect of the lack of

Al atoms in the substrate on the structure of the alumina layer formed. This approach will help to elucidate the actual role played by the presence of Al in the substrate on the alumina structure. Our LEED and STM results show that the unit cell of the alumina film is a sixton, i.e., a rectangle with a $\sqrt{3}$ ratio between the lengths of its two sides. Depending on the tunneling conditions, we have either observed the Al interface atoms, which are arranged in heptagons and pentagons, in the same way as for alumina films on NiAl(110) or on Cu-9 at. % Al(111), or the Ni substrate atoms, which appear to be unaffected by the alumina layer. The specific ratio observed is due to the hexagonal arrangement of oxygen atoms in the interface layer and cannot be ascribed to the influence of the substrate which only drives the domain orientations. We give strong arguments for attributing the same atomic structure to alumina films grown on FeAl(110), NiAl(110), Cu(111), and Cu-9 at. % Al(111). All these superstructures are observed after preparation at high temperature (above 950 K). They correspond to two Al and two O planes but their structure strongly differs from the structures of the different bulk phases of Al_2O_3 . These structures could be the equilibrium state of a two-layer-thick alumina film on a metal. Anyway, it demonstrates that the choice of a substrate for growing alumina films based on the commensurability between a bulk alumina structure and the surface unit cell of the substrate is a too naive consideration.

This result opens perspectives in the preparation of alumina films relevant for many fundamental studies and technological applications, in particular, in the area of oxide-supported metal catalysts since this superstructure could be possibly prepared on many different substrates and not only aluminum-based alloys.

ACKNOWLEDGMENTS

This work has been partially supported by the French National Agency (ANR) in the frame of its Nanoscience Program (PNano, Project Reactgold No. ANR-07-NANO-024-01), and by the C'Nano Program of the Région Ile de France (project REACT-STM-2007).

*Corresponding author; geoffroy.prevot@insp.jussieu.fr

¹H. J. Freund, H. Kuhlenbeck, and V. Staemmler, Rep. Prog. Phys. **59**, 283 (1996).

²R. Franchy, Surf. Sci. Rep. **38**, 195 (2000).

³G. Ertl, H. Knözinger, F. Schüth, and J. Weitkamp, *Handbook of Heterogeneous Catalysis* (Wiley-VCH Verlag GmbH, Weinheim, 2008), Vol. 3.

⁴M. Frank and M. Bäumer, Phys. Chem. Chem. Phys. **2**, 3723 (2000).

⁵M. Bäumer and H. J. Freund, Prog. Surf. Sci. **61**, 127 (1999).

⁶M. Schmid, M. Shishkin, G. Kresse, E. Napetschnig, P. Varga, M. Kulawik, N. Nilius, H. P. Rust, and H. J. Freund, Phys. Rev. Lett. **97**, 046101 (2006).

⁷C. T. Campbell, Surf. Sci. Rep. **27**, 1 (1997).

⁸N. Nilius, M. V. Ganduglia-Pirovano, V. Brazdova, M. Kulawik,

J. Sauer, and H. J. Freund, Phys. Rev. Lett. **100**, 096802 (2008).

⁹P. Gassmann, R. Franchy, and H. Ibach, Surf. Sci. **319**, 95 (1994).

¹⁰V. Rose, V. Podgursky, L. Costina, R. Franchy, and H. Ibach, Surf. Sci. **577**, 139 (2005).

¹¹Y. Jelizova and R. Franchy, Appl. Surf. Sci. **187**, 51 (2002).

¹²P. J. Chen and D. W. Goodman, Surf. Sci. **312**, L767 (1994).

¹³Y. T. Wu, E. Garfunkel, and T. E. Madey, J. Vac. Sci. Technol. A **14**, 2554 (1996).

¹⁴R. Franchy, J. Masuch, and P. Gassmann, Appl. Surf. Sci. **93**, 317 (1996).

¹⁵U. Bardi, A. Atrei, and G. Roviola, Surf. Sci. **268**, 87 (1992).

¹⁶C. Becker, J. Kandler, H. Raaf, R. Linke, T. Pelster, M. Dräger, M. Tanemura, and K. Wandelt, J. Vac. Sci. Technol. A **16**, 1000 (1998).

- ¹⁷G. Kresse, M. Schmid, E. Napetschnig, M. Shishkin, L. Kohler, and P. Varga, *Science* **308**, 1440 (2005).
- ¹⁸K. Müller, H. Lindner, D. M. Zehner, and G. Ownby, *Verh. Dtsch. Phys. Ges.* **25**, 1130 (1990).
- ¹⁹R. M. Jaeger, H. Kuhlenbeck, H.-J. Freund, M. Wuttig, W. Hoffmann, R. Franchy, and H. Ibach, *Surf. Sci.* **259**, 235 (1991).
- ²⁰H. J. Freund and G. Pacchioni, *Chem. Soc. Rev.* **37**, 2224 (2008).
- ²¹G. H. Simon, T. König, M. Nilius, H. P. Rust, M. Heyde, and H. J. Freund, *Phys. Rev. B* **78**, 113401 (2008).
- ²²A. Stierle, F. Renner, R. Streitl, H. Dosch, W. Drube, and B. C. Cowie, *Science* **303**, 1652 (2004).
- ²³E. Napetschnig, M. Schmid, and P. Varga, *Surf. Sci.* **602**, 1750 (2008).
- ²⁴S. Degen, A. Krupski, M. Kraj, A. Langner, C. Becker, M. Sokolowski, and K. Wandelt, *Surf. Sci.* **576**, L57 (2005).
- ²⁵M. Schmid, G. Kresse, A. Buchsbaum, E. Napetschnig, S. Gritschneider, M. Reichling, and P. Varga, *Phys. Rev. Lett.* **99**, 196104 (2007).
- ²⁶S. Le Pévédic, D. Schmaus, and C. Cohen, *Surf. Sci.* **602**, 67 (2008).
- ²⁷S. Le Pévédic, D. Schmaus, and C. Cohen, *Surf. Sci.* **600**, 565 (2006).
- ²⁸W. von Wersin, *Das Buch vom Rechteck: Gesetz und Gestik des Räumlichen* (Otto Maier Verlag, Ravensburg, 1956).
- ²⁹V. Maurice, G. Despert, S. Zanna, M. P. Bacos, and P. Marcus, *Nature Mater.* **3**, 687 (2004).
- ³⁰M. Kulawik, N. Nilius, H. P. Rust, and H. J. Freund, *Phys. Rev. Lett.* **91**, 256101 (2003).
- ³¹N. Nilius, M. Kulawik, H. P. Rust, and H. J. Freund, *Phys. Rev. B* **69**, 121401(R) (2004).
- ³²H. Graupner, L. Hammer, K. Heinz, and D. M. Zehner, *Surf. Sci.* **380**, 335 (1997).